Heliyon 10 (2024) e24339

Contents lists available at ScienceDirect

Heliyon

journal homepage: www.cell.com/heliyon

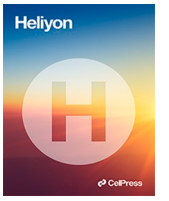

Research article

α-Mangostin suppresses ethanol-induced gastric ulceration by regulating the Nrf2/HO-1 and NF-κB/NLRP3/caspase-1 signaling pathways and gut microbiota

Suqin Yang [a,1], Gang Liu [b,1], Xiankun Xia [a,1], Dali Gan [a], Shijian Xiang [c,*], Meixian Xiang [a,**]

[a] School of Pharmaceutical Sciences, South-Central Minzu University, Wuhan 430074, China
[b] Department of Pharmacy, Renmin Hospital of Wuhan University, Wuhan, China, 430060, Hubei, China
[c] Department of Laboratory Medicine, Renmin Hosipital of Wuhan University, Wuhan, 430060, Hubei, China

ARTICLE INFO

Keywords:
Gastric ulceration
α-Mangostin
Anti-oxidative stress
Anti-inflammation
Autophagy
Nrf2/HO-1 pathway and NF-κB/NLRP3/Caspase-1 pathway

ABSTRACT

α-Mangostin is a natural xanthone derivative isolated from *Camellia atrophy* (CA), commonly known as Lichuan black tea (LBT). The present study investigated the ameliorating effect and mechanism of α-mangostin on alcoholic gastric ulcers (GU) in rats. *In vivo*, α-mangostin relieved pathological symptoms. Moreover, α-mangostin regulated the activation of the nuclear factor (erythroid-derived 2)-like 2 (Nrf2)/heme oxygenase 1 (HO-1) and nuclear factor κB (NF-κB)/NLR family pyrin domain containing 3 (NLRP3)/caspase-1 pathways. Reactive oxygen species (ROS), tumor necrosis factor-α (TNF-α), and interleukin-1β (IL-1β) were significantly decreased and IL-10 were increased, the microtubule-associated protein light chain 3 (LC3)-II/LC3-I ratio was increased, p62 protein expression was decreased, and inducible nitric oxide synthase (iNOS) and cyclooxygenase 2 (COX-2) protein expression was down-regulated. The relevant mechanisms were validated using GSE-1 and RAW264.7 cells in an *in vitro* model. Furthermore, α-mangostin increased *Ligilactobacillus* and *Muribaculum* abundance as well as propionic acid and butyric acid contents. Therefore, α-mangostin possesses antioxidant and anti-inflammatory properties, and remodels intestinal flora dysbiosis through mechanisms that may involve regulation of the Nrf2/HO-1 pathway and NF-κB/NLRP3/caspase-1 pathway. It also increases propionic acid and butyric acid contents. This study provides novel evidence regarding the use of α-mangostin for treating GU.

1. Introduction

Gastric ulcers (GU) is a common gastrointestinal disease affecting approximately 10 % of the global population [1]. Damage to any layer of the stomach may impair normal physiological functions, leading to excessive release of inflammatory factors, nitric oxide synthase (NOS), and reactive oxygen species (ROS) [2]. Excessive use of nonsteroidal anti-inflammatory drugs (NSAID), bacterial

* Corresponding author.
** Corresponding author. School of Pharmaceutical Sciences, South-Central Minzu University, Wuhan, 430074, China.
E-mail addresses: xiangshij3@mail.sysu.edu.cn (S. Xiang), xiangmeixian@mail.scuec.edu.cn (M. Xiang).
[1] Equally contributed to the study.

https://doi.org/10.1016/j.heliyon.2024.e24339
Received 4 August 2023; Received in revised form 7 January 2024; Accepted 8 January 2024
Available online 11 January 2024

infections, excessive alcohol intake, and stress can contribute to stomach ulcers. Binge drinking overstimulates the gastric mucosa, which may lead to gastric mucosa erosion and ulceration in severe cases. Excessive, long-term alcohol consumption can cause GU [3]. GU is a prevalent condition in which the stomach lining is severely damaged [1]. Although patient condition improves with treatment, complete recovery is difficult. Therefore, identifying reliable treatments and medications for GU remains a challenge.

α-Mangostin is a secondary metabolite isolated from Lichuan black tea (LBT) that protects gastric mucosa and is a flavonoid natural product. Several studies have reported that α-mangostin exhibits broadly pharmacological activities, such as antioxidant, antimicrobial, and anti-inflammatory and anticarcinogenic activities [4]. α-Mangostin can reshape visceral adipose tissue inflammation to alleviate age-related metabolic dysfunction in mice. The antioxidant effects of α-mangostin are mainly related to the regulation of antioxidant enzymes, the reduction of oxidative stress markers and increased the expression levels of Nrf2 and HO-1; anti-inflammatory effects of α-mangostin include its modulation of the nuclear factor-κB-related pathway, reduction of pro-inflammatory cytokine levels [5]. Collectively, α-mangostin is a candidate agent for the alleviation of multiple inflammatory conditions and represents a novel therapeutic modality.

To the best of our knowledge, no protective effect of α-mangostin against GU has been reported to date. Therefore, the present study aimed to evaluate the protective effect of α-mangostin on ethanol-induced gastric mucosa injury in rats. Ethanol was used to induce GU in rats because ethanol in the stomach leads to the necrosis of gastric cells and vascular damage, resulting in ulceration. These effects are because of the production of hydroperoxy and superoxide anion radicals during ethanol metabolism in the body [6]. Based on *in vivo* and *in vitro* models, we investigated the anti-inflammatory effect and mechanism of action of α-mangostin, and its potential function in regulating intestinal flora. This study reports a novel therapeutic strategy for the treatment of GU with α-mangostin.

2. Materials and methods

2.1. Materials and reagents

α-Mangostin was purchased from Millipore Sigma (Burlington, MA, USA, MFCD00135200). Ranitidine was obtained from Absin Bioscience (Shanghai, China, abs814762), and GlaxoSmithLine (Brentford, UK). Enzyme-linked immunosorbent assay (ELISA) kits for interleukin (IL)-1β (EMC001b.48), IL-6 (EMC004.48), IL-10 (EMC005.48), and tumor necrosis factor-α (TNF-α) (EMC102a.48) were purchased from Neobioscience Technology (Beijing, China). A prostaglandin E2 (PGE2) ELISA kit was purchased from Elabscience Biotechnology (Houston, TX, USA, E-EL-0034c). Ethanol (95 %) was purchased from Sinopharm Chemical Reagent Co. (Beijing, China, 10009128). An enhanced bicinchoninic acid (BCA) protein assay kit (P0012S), radioimmunoprecipitation assay (RIPA) lysis buffer (P0013), protease and phosphatase inhibitor cocktails for mammalian cell and tissue extracts, and assay kits for superoxide dismutase (SOD) (S0086), water-soluble tetrazolium-8, glutathione (GSH) (S0057S), and malondialdehyde (MDA) (S0131S) were purchased from Beyotime Biotechnology (Shanghai, China).

Antibodies against phosphorylated inhibitor of nuclear factor kappa B (*p*-IκB) kinase alpha subunit (IKKα) (#7355), IKKα (#9242), phosphorylated p65 (p-p65) (#3033), and p65 (#6956) were purchased from Cell Signaling Technology (Danvers, MA, USA). Nuclear factor erythroid 2-related factor 2 (Nrf2) (A1244), p62/sequestosome 1 (A19700), β-actin primary antibodies (AC026), microtubule-associated protein light chain 3 (LC3-II)/LC3-I (A5618), horseradish peroxidase-(HRP) labeled goat anti-rabbit immunoglobulin (Ig)G (AS014), and heme oxygenase 1 (HO-1) (A19062) were purchased from ABclonal Technology (Wuhan, China). Antibodies against COX-2 (GB111037-100), NLR family pyrin domain containing 3 (NLRP3) (GB114320-100), and caspase-1 (GB11383-100), as well as 4 % neutral buffered paraformaldehyde solution (CR2302145) were purchased from Servicebio Biotechnology (Wuhan, China).

GES-1 cells were purchased from Wuhan Sunncell Biotechnology Co., Ltd. (Catalog SNL-304, Wuhan, China), and RAW264.7 cells were purchased from the China Center for Type Culture Collection (CCTCC; Catalog # GDC0143, Wuhan, China). Roswell Park Memorial Institute (RPMI)-1640 medium (SH30027.01), high-dextrose Dulbecco's modified Eagle's medium (DMEM) (SH30243), and phosphate-buffered saline (PBS) (SH30256) were purchased from HyClone (Julich, Germany). Penicillin-streptomycin (15140122), trypsin (25,200,056), and fetal bovine serum (FBS) (26010066) were purchased from Gibco Life Technologies (New York, NY, USA). In addition, 3-(4,5-dimethylthiazol-2-yl)-2,5-diphenyltetrazolium bromide (MTT) (R20227) was purchased from Shanghai YuanYe Biotechnology (Shanghai, China). A microplate reader (Spark 20 M Sunrise) was purchased from Tecan Trading (Shanghai, China). The electrophoresis apparatus, mini-transfer tank, and electrophoresis power supply were obtained from Liuyi Biotechnology (Beijing, China).

2.2. LBT and high-performance liquid chromatography (HPLC) analysis

LBT was purchased from Enshi (Hubei Province, China). LBT (20 g) was extracted thrice using 100 mL of distilled water at 100 °C 3 times for 30 min. The combined solution was filtered, condensed under reduced pressure, and then dissolved in 95 % alcohol to prepare the liquid supernatant. The supernatant was concentrated using a rotatory evaporator and dried in an oven at 40 °C to obtain LBT extracts. The extracts and α-mangostin standard substance (1 and 0.5 mg/mL, respectively) were diluted into methanol for HPLC analysis. The chromatographic analysis was performed using a reverse-phase Nucleosil C18 column (Dionex-Ultimate, series 3000, USA, 4.6 × 250 mm, 5 μm). The mobile phase consisted of an acetonitrile (Aladdin, Shanghai, China):0.1 % H_3PO_4 in water (70:30) mixture processed for 45 min at a flow rate of 0.2 mL/min. The temperature of the column oven was set to 30 °C. The injection volume was 10 μL and the detection wavelength was set at 280 nm [7]. The results of the HPLC analysis are shown in Supplementary Fig. S1. The LBT and α-mangostin sample (15.2 % of total flavonoids) had the same absorption peak at the same retention time.

2.3. Animals and groups

All animal procedures were performed according to the National Institutes of Health (NIH) Guide for the Care and Use of Laboratory Animals. Sixty male Sprague-Dawley (SD) rats (6 weeks old, 180 ± 20 g) were obtained from the Liaoning Provincial Laboratory Animal Resource Center (license no: SCXK [Liaoning] 2020–01). Animals were kept in a specific pathogen-free (SPF) animal laboratory under a 12 h light/dark cycle at a room temperature of 20–25 °C (humidity, 45–75 %). The rats were randomly divided into six groups of ten mice each: negative control, model, low (L)-dose, medium (M)-dose, and high (H)-dose (32, 64, and 96 of α-mangostin, respectively) groups. The positive control group was treated with ranitidine (50 mg/kg). Each group was administered α-mangostin once daily for 7 d with α-mangostin suspended in 0.9 % saline. Additionally, based on translating the doses from animal to human studies through body surface area conversion, the doses of 32, 64, and 96 mg/kg α-mangostin that we administered to the rats.

2.4. Animal experiments

The rats were fasted for 24 h and provided free access to water for 2 h before experimentation. Excluding the control group (administered 0.9 % saline, 5 mL/kg), the GU model was established in all groups through intragastric administration of 95 % ethanol (5 mL/kg). Rats were euthanized under ether anesthesia 1 h after being administered 95 % ethanol.

Blood samples were collected and centrifuged at 800×*g* for 10 min at room temperature, and serum was stored at −80 °C for subsequent analysis. The gastric tissues of rats were washed with 0.9 % saline, photographed, frozen using liquid nitrogen, and stored at −80 °C. The area of the mucosal GU was determined using ImageJ software (National Institutes of Health, Bethesda, MD, USA). Gastroprotection was estimated using the following formula based on the inhibition rate (I%), where UA denotes the ulcerated area [8].

$$I\% = [(UA_{\text{model group}} - UA_{\text{treatment group}})/UA_{\text{model group}}] \times 100\%$$

2.5. Histopathology and periodic acid and schiff (PAS) staining [9]

The gastric tissues were fixed in 4 % paraformaldehyde for 48 h, then embedded in paraffin and cut into 4-μm thick sections. The gastric tissues were then stained with hematoxylin and eosin (H&E). The pathological changes were evaluated using a digital screen microscope and the following formula: $I\% = [(\text{score}_{\text{model group}} - \text{score}_{\text{treatment group}})/\text{score}_{\text{model group}}] \times 100$ %.

The deparaffinized tissue sections were immersed in periodic acid and PAS solution for 10 min. Gastric tissue samples were analyzed using a light microscope (AE2000; Motic, Hong Kong, China). The mucosal index was used to estimate the damage as through the following formula: mucosal index (%) = $(\text{area}_{\text{acidic mucus}} + \text{area}_{\text{neutral mucus}})$/total area.

2.6. Cell assay

RAW264.7 cells were cultured in high-dextrose DMEM supplemented with 10 % FBS, 1 % penicillin, and 1 % streptomycin. The cells were then placed in a cell incubator at 37 °C in an atmosphere containing 5 % CO_2. Cells were inoculated in 96-well plates (1.0×10^4 cells/well) overnight. Then, various concentrations of α-mangostin solution (0, 0.4, 0.8, 1, 2, 4, 8, 10, 20, 40, or 80 μM) in DMEM without FBS were added to the cells for 24 h. After washing with PBS, 10 μL of MTT solution was added for 4 h incubation. Then, we discarded the medium and added 150 μL of dimethyl sulfoxide (DMSO) to lyse the crystals. Optical density (OD) was measured at 490 nm. Cells were divided into five groups for cellular experiments, including the control group treated with DMEM only, the LPS group treated with lipopolysaccharide (LPS; 100 ng/mL) only, and the other three groups treated with LPS (100 ng/mL) with α-mangostin (10, 20, or 40 μM) [10].

GES-1 cells were cultured in RPMI-1640 medium supplemented with 10 % FBS, 1 % penicillin, and 1 % streptomycin. GES-1 cells were cultured and treated as the same as RAW264.7 cells. Cells were divided into five groups, including the control group treated with RPMI-1640 medium only, the ethanol group treated with 1 % ethanol only, and the other three groups treated with 1 % ethanol with α-mangostin (10, 20, or 40 μM).

Cell supernatants were collected to determine the relevant cytokine levels. The expression of relevant proteins in the cells was also measured.

2.7. Measurement of ROS levels

Fresh gastric tissues were frozen in liquid nitrogen and cut into 4-μm slices. The tissue slices were incubated with an autofluorescence quencher for 5 min and then washed for 10 min. Slices were incubated with ROS staining solution in an incubator at 37 °C for 30 min. Next, the slices were immersed in 4',6-diamidino-2-phenylindole solution for 10 min. The cells were observed using a fluorescence microscope (ECLIPSE Ti2; Nikon, Japan). The mean fluorescence intensity of ROS was determined using ImageJ software [11].

2.8. Determination of SOD, MDA, and GSH levels

Fresh gastric tissue was collected and homogenized on ice with 5 mL of 5 % trichloroacetic acid (TCA) per gram. Next, the homogenate was centrifuged at 4 °C for 15 min at 1000×*g*. The supernatant was collected and the SOD, MDA, and GSH levels were determined using a kit, according to the manufacturer's instructions [12].

2.9. Determination of cytokine levels

The supernatants of the tissue homogenates were collected, and the levels of inflammatory cytokines, including PGE2, IL-10, IL-6, IL-1β, and TNF-α [13], were analyzed according to the manufacturer's instructions for the kits.

2.10. Western blot analysis

Total protein in the gastric tissue was extracted using NP-40 lysis buffer containing a mixture of protease and phosphatase inhibitors (50:1). Protein concentration was measured using a BCA protein quantification kit. The proteins were separated using 10 % sodium dodecyl-sulfate-polyacrylamide gel electrophoresis (SDS-PAGE), transferred to polyvinylidene fluoride (PVDF) membranes for 1.5 h, sealed with 5 % skim milk for 1 h, then washed thrice with tris-buffered saline with Tween 20 (TBST). Then, the PVDF membranes were incubated with primary antibodies (Supplementary Table 1) at 4 °C in a refrigerator overnight and then incubated with secondary antibodies for 1 h. The PVDF membranes were washed thrice with TBST, and the target proteins were detected using ECL reagent and quantified using the ImageJ software (NIH Image, USA) [14].

2.11. Sequencing of the bacterial 16S rRNA gene

An intestinal flora imbalance is an important pathological factor in ethanol-induced GU [15]. Therefore, 16S rRNA gene sequencing was used to evaluate α-mangostin regulation of the intestinal flora in ethanol-induced GU. Bacterial DNA in the feces of each group was

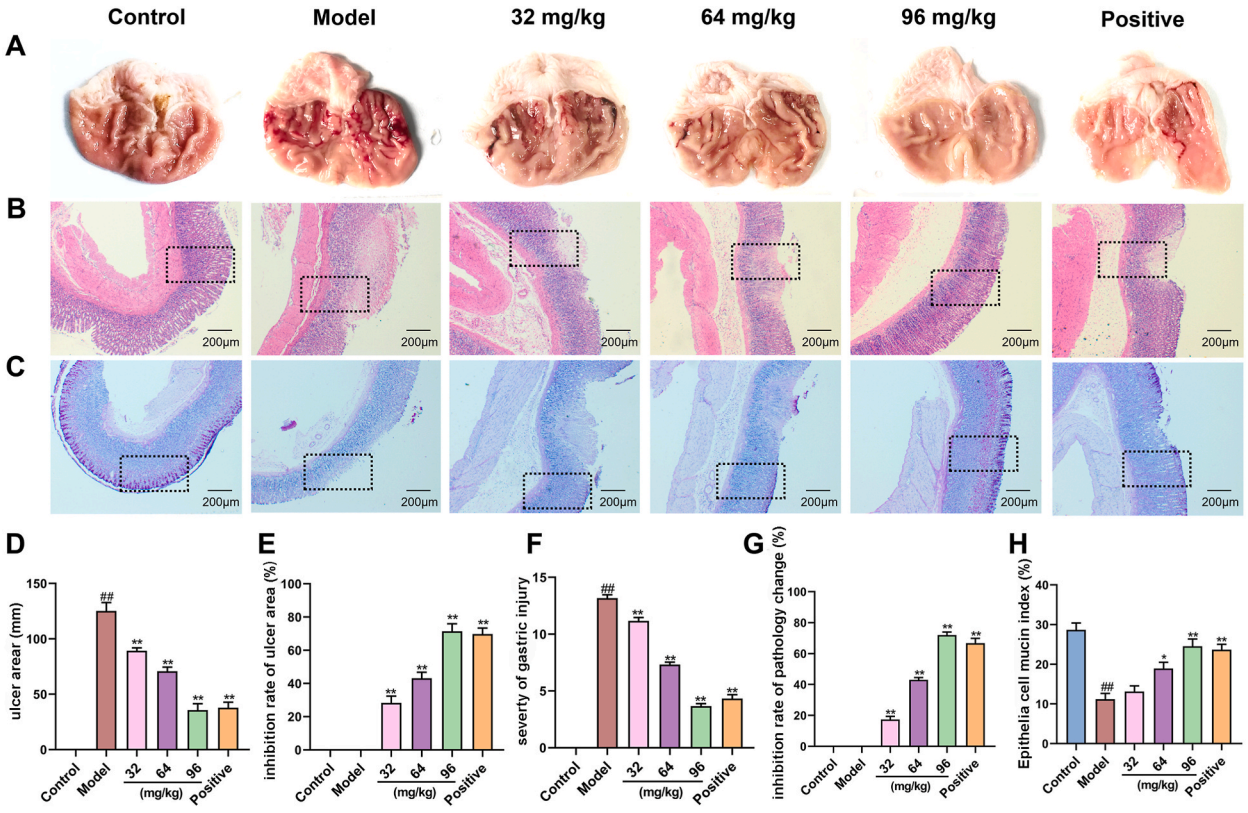

Fig. 1. α-Mangostin protected the gastric mucosa of rats macroscopically and microscopically. (A) Macroscopic photographs of gastric tissue. (B) H&E staining of gastric sections from rats (magnification × 200). (C) PAS staining of gastric sections from rats (magnification × 200). (D) Ulcerated area in the gastric mucosa of rats. (E) Evaluation of percent inhibition of the area of a gastric mucosa ulcer by α-mangostin. (F) Pathological evaluation using H&E staining. (G) Evaluation of percent inhibition of gastric mucosa pathological changes by α-mangostin. (H) The Mucosa Index based on PAS staining. Data are the mean ± SEM. $^{\#\#}P < 0.01$ *vs*. Control group; $^{*}P < 0.05$ and $^{**}P < 0.01$ *vs*. Model group, n = 6.

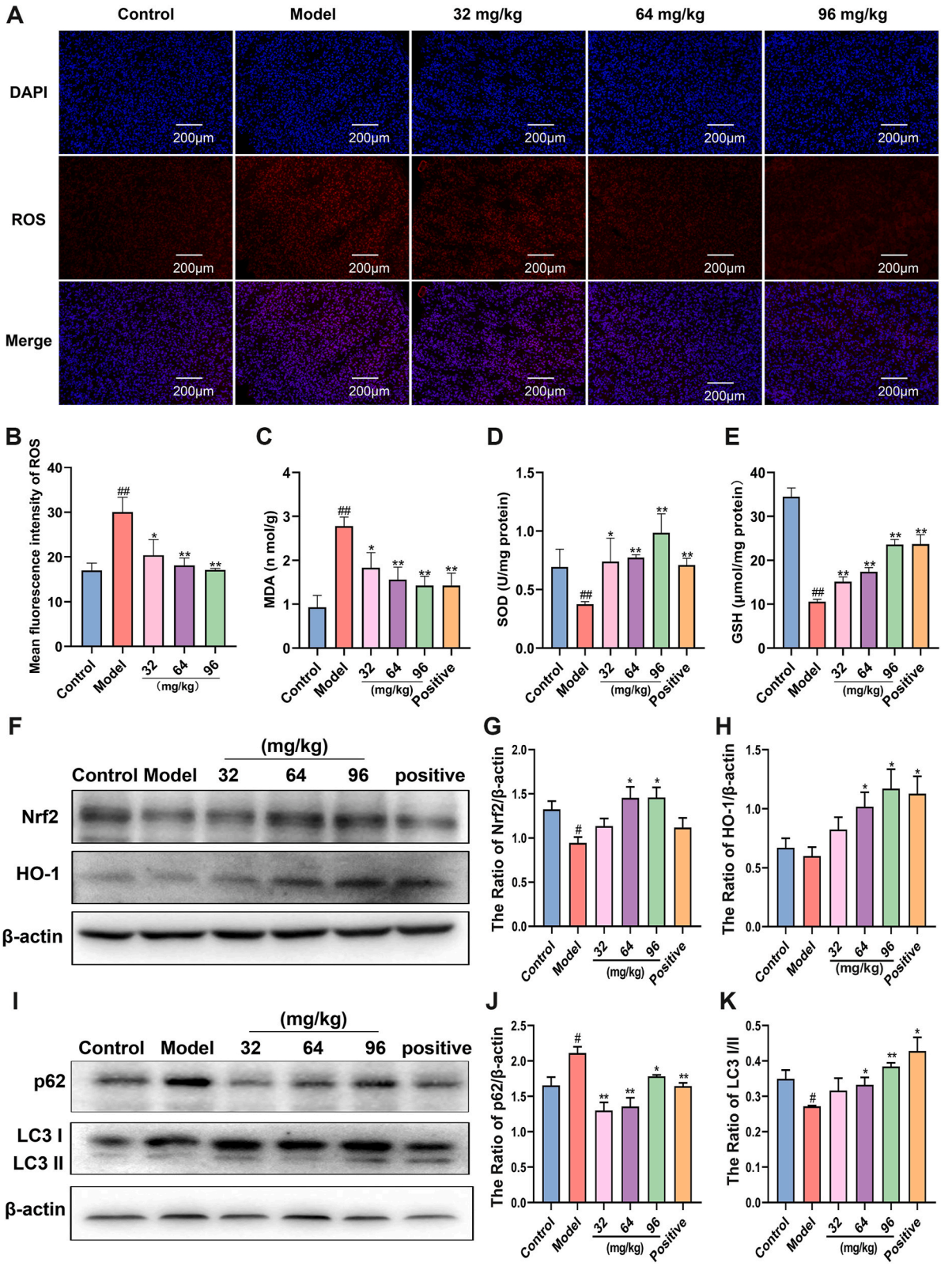

(caption on next page)

Fig. 2. α-Mangostin reduced oxidative stress and regulated autophagy in gastric tissue. (A) ROS levels in gastric tissue. (B) Semiquantitative image analysis of ROS levels in tissue. (C) Effects of α-mangostin on the levels of MDA. (D) Effects of α-mangostin the levels of SOD. (E) Effects of α-mangostin on the levels of GSH. (F) Representative western blotting images of Nrf2 and HO-1 protein expression. (G–H) The expressional changes of Nrf2/β-actin and HO-1/β-actin proteins. (I) Representative western blotting images of p62, LC3-II, and LC3-I protein expression, β-actin protein was the loading control. The figure shows data from one of the 3 independent experiments. (J–K) The expressional changes of p62/β-actin ratio and LC3-II/LC3-I ratio. Data are the mean ± SEM. $^{\#\#}P < 0.01$ *vs*. Control group; $^{*}P < 0.05$ and $^{**}P < 0.01$ *vs*. Model group, n = 3.

extracted using a DNA Kit (MN NucleoSpin 96 Soi), according to the manufacturer's instructions. The quality of the DNA samples was determined before they were used for library construction, and the primers 515F (5′-GTGYCAGCMGCCGCGGTAA-3′) and 806 R2 (5′-GGACTACNVGGGTWTCTAAT-3′) were used to amplify the V4 hypervariable variable region of the bacteria. The polymerase chain reaction (PCR) amplification products were purified using the OMEGA DNA purification columns. The 16S rRNA gene V4 was sequenced using an Illumina NovaSeq 6000 platform (Beijing Baimaike Biotechnology Co., Ltd., Beijing, China). The raw data for each sample were spliced using FLASH software (version 1.2.11), and low-quality reads were filtered to clean the data [16]. The consensus sequence was obtained through stitching (Trimmomatic, version 0.33), whereas chimeras (UCHIME, version 8.1) were eliminated to obtain high-quality tag sequences. USEARCH (version 10.0) was used to cluster 97 % of clean tags into operational taxonomic units (OTU). Representative OTU sequences were classified using the Ribosomal Database Project (RDP) Classifier (version 2.2) at a confidence threshold of 0.8. α and β diversities were analyzed using QIIME software (version 2.0). β diversity was calculated as inter-sample distances using the unweighted unifrac algorithm to determined differences between samples and principal coordinates analysis (PCoA) plots were produced using R software (version 4.1.0). Finally, significant differences between groups at the phylum and genus levels were analyzed using Metastats (http://metastats.cbcb. umd.edu/).

2.12. Analysis of short-chain fatty acids (SCFAs) using gas chromatography (GC)

To determine the contents of SCFAs, 100-mg fecal samples were collected in 2-mL centrifuge tubes, 100 μL methanol was added, and the tubes were centrifuged for 10 min at 12,000×*g* at 4 °C. Supernatant (100 mL) was placed into new 2-mL centrifuge tubes, mixed with 25 % metaphosphoric acid at a 5:1 ratio, and stored overnight at 4 °C. Next, the samples were centrifuged for 10 min at 12,000×*g* at 4 °C. The SCFA contents were analyzed using GC (TRACE 1300, Thermo Fisher Scientific, USA) with a TR-FAME column (60 m × 0.25 mm, ID × 0.25 μm). The detection temperature was 230 °C, the sample volume was 1 μL, and the carrier gas was nitrogen at a flow rate of 3 mL/min [17].

2.13. Statistical analyses

All data are presented as the mean ± standard error of the mean (SEM). The SPSS 9.0 software (IBM, Armonk, NY, USA) was used to analyze the results. Image-Pro Plus (version 6.0; Media Cybernetics, San Diego, CA, USA) and ImageJ software were used to analyze the histological and fluorescent images. GraphPad bar graphs were generated using Prism 8.0.2 (GraphPad, La Jolla, CA, USA). Statistical significance was set at $p < 0.05$ and $p < 0.01$.

3. Results

3.1. α-Mangostin relieved symptoms of GU in ethanol-induced rats

In the GU rat model, the macroscopic images showed that ethanol resulted in serious GU symptoms, which could be reversed by various concentrations of α-mangostin (Fig. 1A). The H&E and PAS staining results confirmed that α-mangostin significantly reduced the hemorrhaging in the inner lining of the stomach and the GU area, and improved mucosal erosion in the treatment groups compared with that in the model group, in a dose-dependent manner (Fig. 1B and C). Pathological evaluation further emphasized that ulcer area, inhibition of ulcer area, severity of gastric injury, inhibition of pathology change, and the epithelial cell mucin index were alleviated following α-mangostin treatment (Fig. 1D). These results indicate that α-mangostin could alleviate ethanol-induced GU in a dose-dependent manner.

3.2. α-Mangostin inhibited the oxidative stress reaction and regulated Nrf2/HO-1 expression and autophagy in GU tissues

Excessive alcohol stimulation causes excessive production of ROS, disrupting oxidative homeostasis in the gastric tissue. The Nrf2/HO-1 signaling pathway has recently been reported to contribute significantly to the attenuation of lipid peroxidation in several organs and pathological injuries [18,19]. Therefore, we investigated the ROS levels in the gastric tissues of various treatment groups. The immunofluorescence (IF) results showed that alcohol stimulation increased the ROS levels, whereas α-mangostin treatment markedly reduced the ROS levels in a dose-dependent manner, which was similar to that in the positive group (Fig. 2A and B). ELISA results showed that alcohol induction significantly increased MDA levels and reduced GSH and SOD levels in the model group, and that α-mangostin reversed this trend (Fig. 2C–E). α-Mangostin alleviated alcohol-induced oxidative stress in the gastric tissues. To further explore the antioxidant mechanism of action of α-mangostin, the expression levels of Nrf2 and HO-1 were determined; both were notably down-regulated in the model group, and this was reversed by α-mangostin treatment **(**Fig. 2**F–H)**.

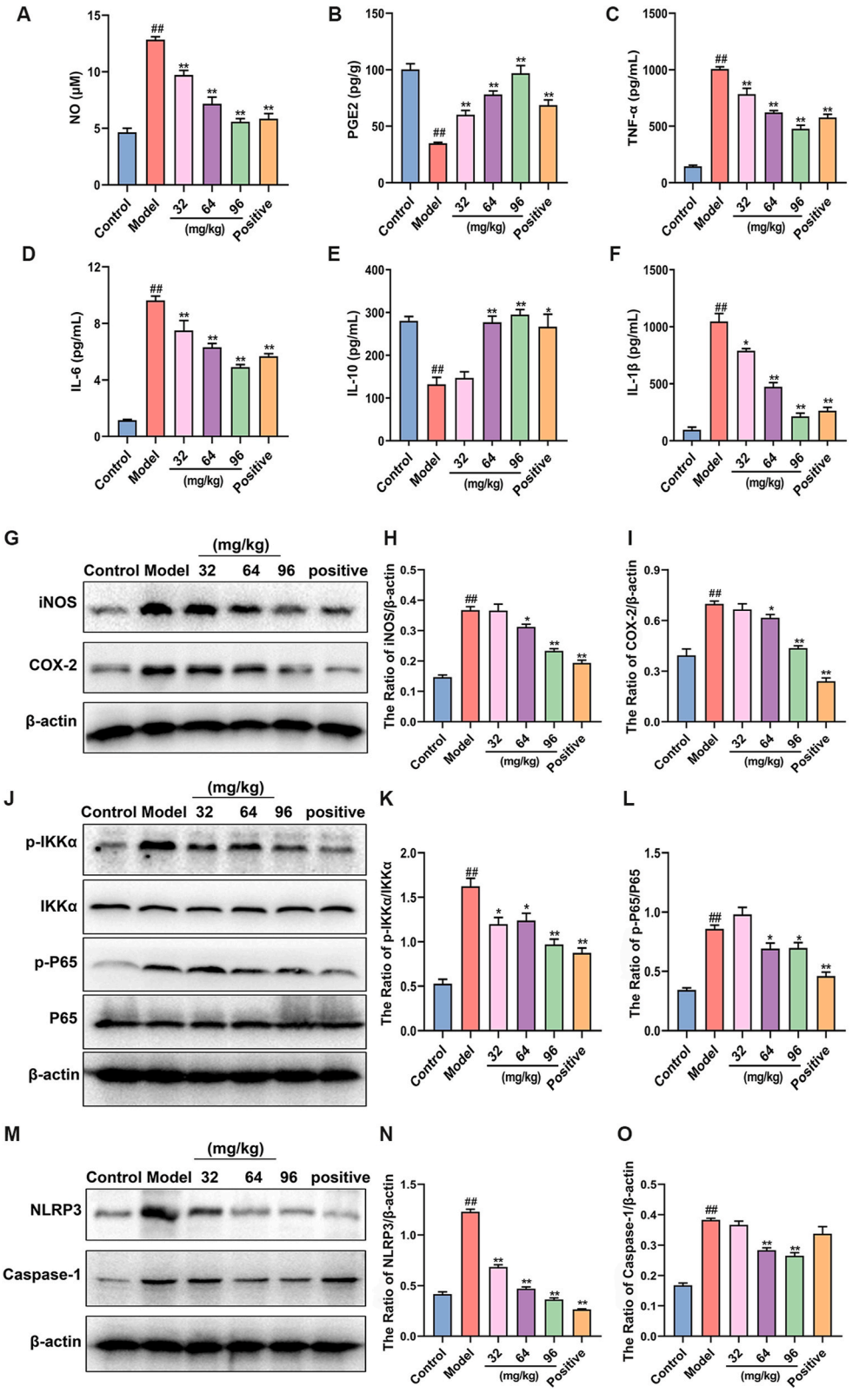

(caption on next page)

Fig. 3. α-Mangostin suppressed release of pro-inflammatory cytokines and expression of related signal pathways in gastric tissue. (A) The level of NO. (B) the level of PGE_2. (C) the level of TNF-α. (D) the level of IL-6, (E) the level of IL-10. (F) the levels of IL-1β. (G) Representative western blotting images of iNOS and COX-2 protein expression, β-actin protein was the loading control. (H–I) The expressional changes of the ratio of iNOS/β-actin and COX-2/β-actin proteins. (J) Representative western blotting images of *p*-IKKα, IKKα and p-p65, p65 protein expression, β-actin protein was the loading control. (K–L) The expressional changes of the ratio of *p*-IKKα/IKKα and p-p65/p65 protein. (M) Representative western blotting images of NLRP3 protein and Caspase-1 protein. (N–O) The expressional changes of the ratio of NLRP3/β-actin and Caspase-/β-actin 1, β-Actin protein was the loading control. Data from one of three independent experiments are shown. Data are the mean ± SEM. $^{\#\#}P < 0.01$ *vs*. Control group; $^{*}P < 0.05$ and $^{**}P < 0.01$ *vs*. Model group, n = 3.

Excessive alcohol intake causes inflammatory damage in the gastric tissue and is accompanied by characteristic cellular autophagy; therefore, we explored the expression levels of autophagy-related proteins p62 and LC3 in each group using western blotting. Compared with the control group, LC3-II protein levels were reduced and p62 protein levels were increased in the model group **(**Fig. 2**I–K)**. Interestingly, α-mangostin promoted the transformation from LC3-I to LC3-II, increased the LC3-II/LC3-I ratio, and reduced p62 protein expression. This indicates that α-mangostin could alleviate oxidative damage by regulating Nrf2/HO-1 expression and autophagy in GU tissues.

3.3. α-Mangostin suppressed the inflammatory response by inhibiting activation of iNOS/COX-2 and the NF-KB/NLRP3/caspase-1 signaling pathway in GU tissues

An exaggerated inflammatory state is a major symptom and a key driver of GU, and manifests through an imbalance in immune cell phenotypes and secretory functions. We detected the related inflammatory factors in GU tissues using ELISA. Compared with that of the control group, the expression levels of TNF-α, IL-6, IL-1β, PGE2, and NO were increased, and that of IL-10 was reduced in the model group (Fig. 3A–F). Interestingly, α-mangostin reversed these inflammatory factors to protect GU tissues from inflammatory injury. Furthermore, western blotting results showed that iNOS and COX-2 expression increased significantly in ethanol-induced GU tissues (Fig. 3G–I). However, α-mangostin treatment significantly down-regulated iNOS and COX-2 expression.

The massive release of TNF-α, IL-6, and IL-1β is closely related to NLRP3 and NF-κB signaling pathway activation; therefore, we analyzed the expression of NLRP3, caspase-1, and the vital proteins of the NF-κB pathway. The expression ratios of *p*-IKKα: IKKα and p-p65: p65 were significantly increased in the model group, whereas α-mangostin treatment significantly reduced the expression of these proteins in the treated groups (Fig. 3J-L). In addition, α-mangostin treatment significantly down-regulated NLRP3 and caspase-1 expression in a dose-dependent manner (Fig. 3M − O). Therefore, α-mangostin may reduce NO and PGE2 by suppressing iNOS and COX-2 expression. Moreover, α-mangostin suppressed the activity of the NF-κB signaling pathway and downstream NLRP3 and caspase-1.

3.4. α-Mangostin inhibited oxidative stress by activating the Nrf2/HO-1 pathway and regulated autophagy in GES-1 cells

To further support the *in vitro* protective role of α-mangostin, ethanol-induced GES-1 cells were established as an oxidative stress model. We used 10, 20, and 40 μg/mL as the α-mangostin concentrations, as determined using the MTT assay **(**Supplementary Fig. S2**). In contrast with the control group, expressions of Nrf2 and HO-1 were decreased in ethanol-treated cells, whereas pre-treatment with α-mangostin significantly increased the expression of these proteins (**Fig. 4A–C**)**. These results illustrate that α-mangostin inhibited oxidative stress *in vitro* by activating the Nrf2/HO-1 signaling pathway. Furthermore, ethanol treatment significantly reduced the LC3-II:LC3-I ratio and increased p62 levels (Fig. 4D–F). α-Mangostin treatment reversed this phenomenon, indicating that α-mangostin could regulate cell autophagy to exert anti-inflammatory effects. Importantly, α-mangostin reduced MDA and H_2O_2 levels and increased SOD and GSH levels in ethanol-treated cells (Fig. 4G–J). Therefore, α-mangostin reduced ethanol-induced oxidative stress by regulating SOD, MDA, H_2O_2, and GSH levels. These results are consistent with those of previous *in vivo* experiments.

3.5 α-Mangostin inhibited the inflammatory response by inhibiting the iNOS/COX-2 and the NF-KB/NLRP3/caspase-1 signaling pathwasy in RAW264.7 cells.

To further support our findings regarding the anti-inflammatory mechanisms of α-mangostin *in vitro*, LPS-induced RAW264.7 cells were established as an inflammation model. As previously, 10, 20, and 40 μg/mL was selected as the α-mangostin treatment concentrations. In LPS-treated RAW264.7 cells **(**Supplementary Fig. S2**), α-mangostin inhibited the protein expression of iNOS, COX-2 (**Fig. 5A–C), NLRP3, and caspase-1 (Fig. 5D–F), and down-regulated the *p*-IKKα:IKKα and p-p65:p65 ratios (Fig. 5G–I). These western blotting results demonstrate that α-mangostin possessed the ability to inhibit the inflammatory response *in vitro* by suppressing the expression of iNOS, COX-2, NLRP3, and caspase-1, and inhibiting activation of the NF-κB pathway.

Moreover, as shown in Fig. 5J-O, NO, PGE2, TNF-α, IL-1β, and IL-6 expression was significantly upregulated, whereas the IL-10 was significantly down-regulated after LPS stimulation. However, α-mangostin reversed these changes. Therefore, α-mangostin dose-dependently inhibited the LPS-stimulated inflammatory response *in vitro*.

3.5. α-Mangostin regulated intestinal flora dysbiosis and promoted the production of SCFAs in ethanol-induced GU models

16S rRNA gene sequencing was performed to analyze the regulation of α-mangostin on the diversity and composition of the colonic microbiota in ethanol-induced GU. The Chao and Shannon indices reflect species abundance and diversity and are important indicators

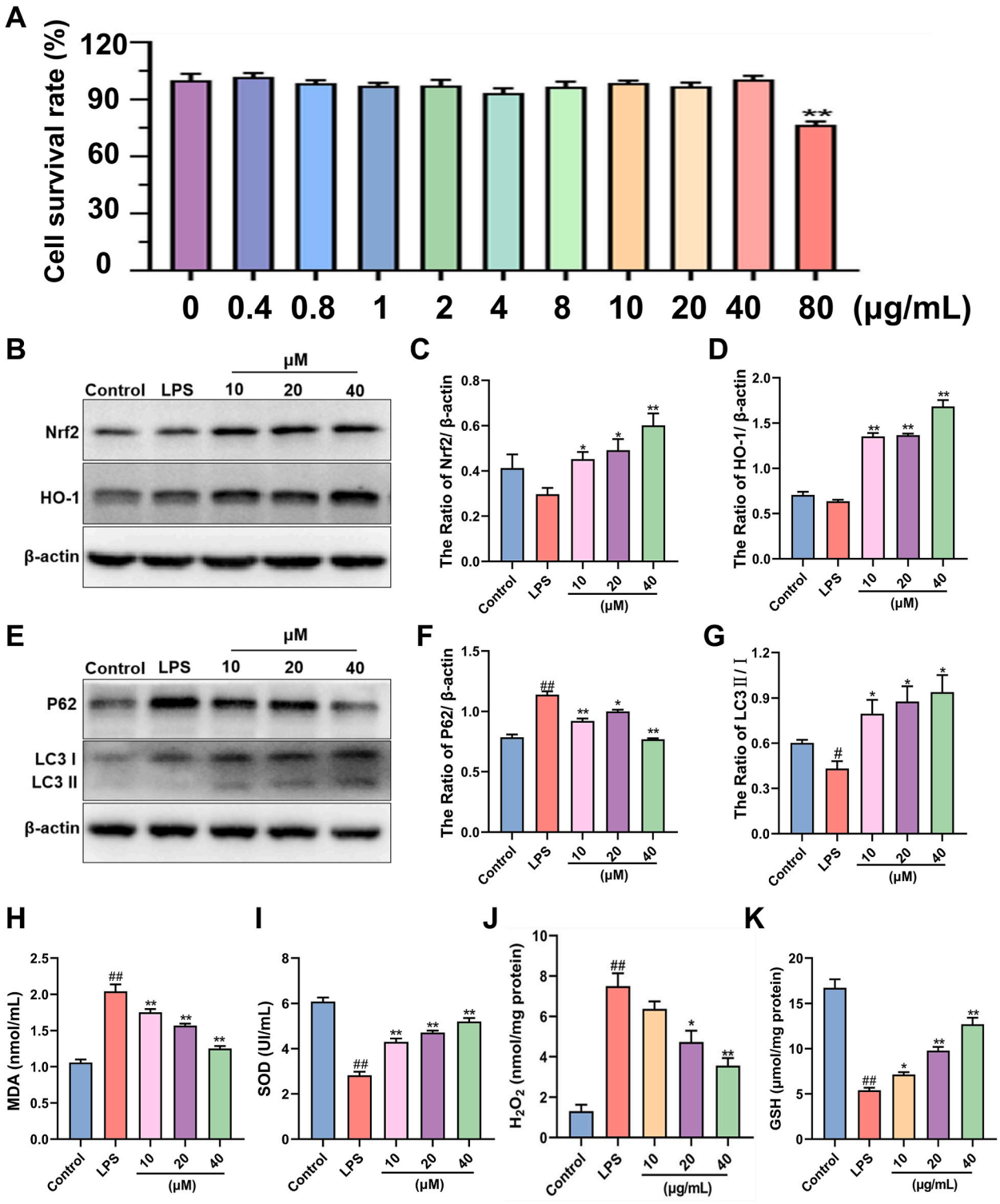

Fig. 4. α-Mangostin reduced oxidative stress and regulated autophagy in GSE-1 cells. (A) Representative western blotting images of Nrf2 and HO-1 protein expression. (B–C) The expressional changes of the ratio of Nrf2/β-actin and HO-1/β-actin. (D) Representative western blotting images of p62, LC3-II, and LC3-I, β-actin protein was the loading control. (E–F) The expressional changes of the ratio of p62/β-actin and LC3-II/LC3-I proteins. (G) The level of MDA. (H) The level of SOD. (I) The level of H_2O_2. (J) The level of GSH, data from one of three independent experiments are shown. Data are the mean ± SEM. $^{\#\#}P < 0.01$ *vs.* Control group; $^{*}P < 0.05$ and $^{**}P < 0.01$ *vs.* Model group, n = 3.

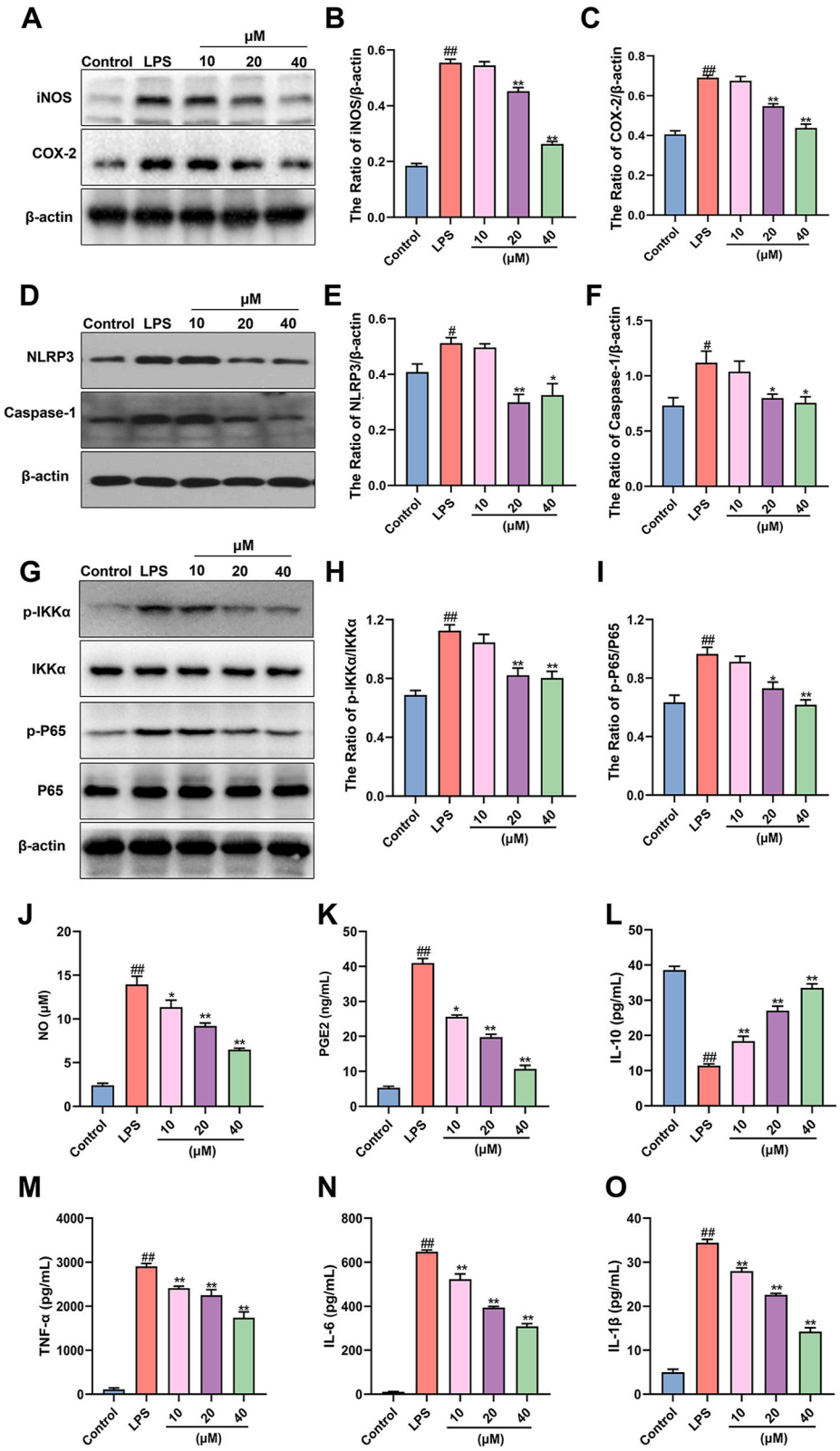

(caption on next page)

Fig. 5. α-Mangostin suppressed LPS-induced release of proinflammatory cytokines and expression of related signal pathways in RAW264.7 cells. (A) Representative western blotting images of iNOS and COX-2; β-actin protein was the loading control. Data from one of three independent experiments are shown. (B–C) The expressional changes of the ratio of iNOS/β-actin and COX-2/β-actin. (D) Representative western blotting images of NLRP3 protein and Caspase-1 protein. (E–F) The expressional changes of the ratio of NLRP3/β-actin and Caspase-1/β-actin. (G) Representative western blotting images of *p*-IKKα, IKKα and p-p65, p65 protein expression, β-actin protein was the loading control. (H–I) The expressional changes of the ratio of *p*-IKKα/IKKα and p-p65/p65 protein. (J) The level of NO. (K) The level of PGE_2. (L) The level of IL-10. (M) The level of TNF-α. (N) The level of IL-6. (O) The level of IL-1β. Data from one of three independent experiments are shown. Data are the mean ± SEM. $^{\#\#}P < 0.01$ *vs*. Control group; $^{*}P < 0.05$ and $^{**}P < 0.01$ *vs*. Model group, n = 3.

of α-diversity. In ethanol-induced GU **models,** alcohol stimulation decreased the Chao and Shannon indices compared to that of the control group (Fig. 6A and B). However, α-mangostin treatment increased the Chao index. The β-diversity was assessed using PCoA, which was based on the binary_jaccard statistical algorithm, and it was found that the intestinal microbiota species significantly differed between the control, model, and α-mangostin-treated groups (Fig. 6C). The results of the 16S rRNA analysis demonstrated that the dominant bacteria were *Bacteroidetes*, *Firmicutes*, *Campylobacterota*, and *Spirochaetota*, and the dominant genera were unclassified_*Muribaculaceae* and unclassified_*Lachnospiraceae* (Fig. 6D). At the genus level, α-mangostin treatment enhanced the abundance of beneficial bacteria, such as *Ligilactobacillus*, *Muribaculum,* and *Lachnospiraceae*_UCG_010 (Fig. 6E). In addition, α-mangostin decreased the abundance of *Rikenellaceae*_RC9_gut_group, *Oscillibacter*, and GCA_900,066,575 (Fig. 6F).

Linear discriminant analysis Effect Size (LEfSe) analysis was used to identify statistically significant biomarkers in the different groups to identify the dominant microorganisms. The numbers of specific taxa in the control, model, and α-mangostin-treated groups were eleven, nine, and six, respectively (Supplementary data Fig. S3). Moreover, linear discriminant analysis (LDA) was performed to distinguish bacterial taxa and showed significant differences (LDA score ≥4). The dominant taxa in the control group were f_*Muribaculaceae* and s-unclassified *Muribaculaceae*. The dominant taxa in the model group were g_*Bacteroides* and f_*Bacteroidaceae*. The dominant taxa in α-mangostin group were g_*Akkermansia* and o_*Verrucomicrobiales* (Supplementary Fig. S3). Therefore, α-mangostin partially ameliorated the dysregulation of intestinal microbiota in ethanol-induced GU.

SCFAs are the primary metabolites of intestinal bacteria and are considered mediators of intestinal immune function regulation by the gut microbiota. Clinical studies have verified that SCFAs play an important role in regulating immunity and inflammation [20]. Therefore, we determined SCFA content using GC. Notably, α-mangostin treatment significantly increased the content of total SCFAs and especially the contents of propionic acid and butyric acid (Fig. 6G–I).

3.6. Correlation analysis of GU, oxidative stress, inflammation, and autophagy

The correlation analysis of heatmap from GU models showed that Nrf2 and HO-1 expression was positively correlated with GSH level, SOD level, propionic acid content, butyric acid content, and the LC3-II/LC3-I expression ratio, and was negatively correlated with ROS, MDA, NO, PGE2, IL-1β, IL-6, and TNF-α, as well as the expression of p62, iNOS, COX-2, p-P65, IKKα, NLRP3, and caspase-1. In addition, the expression levels of iNOS, COX-2, p-P65, IKKα, NLRP3, and caspase-1 were positively correlated with the ROS, MDA, NO, PGE2, IL-1β, IL-6, TNF-α, and p62, but were negatively correlated with GSH and SOD activity, the LC3-II/LC3-I expressions ratio, Nrf2 and HO-1 protein expression, and the propionic acid and butyric acid contents (Supplementary Fig. S4).

4. Discussion

GU is a common gastric injurious disease and can be triggered by various factors, such as alcohol consumption, smoking, irritation-causing foods and drugs, and physical stress [21]. An imbalance between the erosive effects of gastric acid and pepsin and the defenses, such as PGs, NO, and growth factors in the gastric mucosa, results in a weakening of the self-protective barrier of the gastric mucosa. Subsequent damage through erosion results in the formation of GU [22]. The progression of GU is accompanied by immune dysfunction and intestinal flora disorders, which exacerbate the ulcerative response. Thus, safe and effective drugs are required to treat GU [23]. α-mangostin, a bioactive flavonoid in LBT, has been shown to possess antioxidant and anti-inflammatory properties and is used as an intervention and adjunctive therapy for a broad range of inflammatory diseases. In the present study, we investigated the protective role of α-mangostin in resistance to ethanol-induced GU, and the mechanisms involved, which may be related to antioxidant, anti-inflammatory, autophagy modulation, and intestinal flora homeostasis effects.

In this study, an ethanol-induced GU rat model was used, which showed hemorrhage, edema, necrosis, and inflammation [24]. Mechanistically, ethanol stimulation induces excessive ROS production in gastric tissues, and ROS damage the gastric mucosa [25]. During this process, indicators related to redox reactions, including MDA, SOD, GSH, and MPO, reflect the oxidative stress status of gastric injury to some extent [19]. Our results showed that α-mangostin significantly alleviated ethanol-induced GU symptoms through a reduction in bleeding in the gastric lining and GU area as well as an improvement in mucosal erosion in the histologic evaluation of the gastric mucosa. Moreover, ethanol induction significantly increased ROS, MDA, and MPO levels and decreased SOD and GSH levels, a phenomenon that was reversed by α-mangostin. These findings strongly suggest a protective effect of α-mangostin on gastric tissues, which was consistent with previously reported antioxidant mechanisms [26]. ROS overproduction is closely associated with autophagy activation and inflammation [27]. LC3-II is a core protein in autophagy, and p62 can deliver ubiquitinated proteins to autophagosomes for degradation [28]. α-Mangostin treatment increased the LC3-II protein expression and reduced the p62 protein expression. This result emphasizes that α-mangosteins may alleviate ethanol-induced GU by regulating autophagy reaction. PGE2 maintained epithelial cell integrity, improved mucosal blood flow, and acted as a gastric protectant [29]. Ethanol-induced GU was

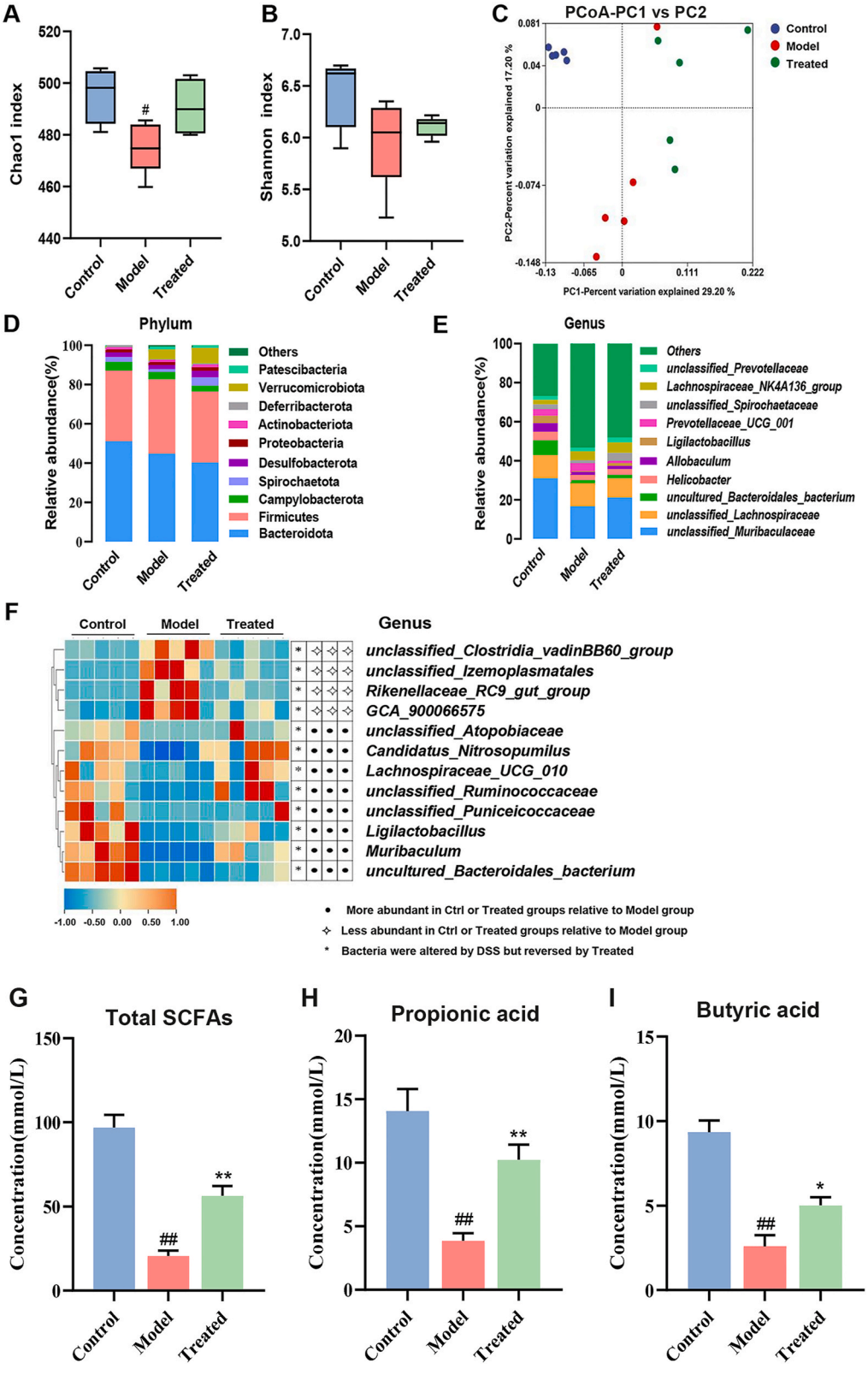

(caption on next page)

Fig. 6. α-Mangostin alleviated the dysbiosis of intestinal flora and promoted the secretion of SCFAs in rat. (A) The result of Chao index. (B) The result of Shannon index. (C) Principal Coordinates Analysis (PCoA) for β-diversity. (D) Differences of gut microbial at the phylum level. (E) Changed in intestinal microbiota composition at phylum and genus levels from different groups. (F) Heat map at the genus level. (G) Statistical results of total SCFAs. (H) Statistical results of propionic acid. (I) Statistical results of butyric acid. All data were represented as mean ± SEM (n = 3). $^{\#}p < 0.05$ and $^{\#\#}p < 0.01$ versus Control group. $^{*}p < 0.05$ and $^{**}p < 0.01$ versus the ethanol stimulation group.

associated with a significant reduction in the content of PGE2, whereas α-mangostin increased the PGE2 content and suppressed the expression of COX-2 protein and iNOS protein.

The transcription factor Nrf2 plays a key role in the cellular defense mechanism by maintaining the antioxidant status and participates in HO-1 transcription [30]. Nrf2 could promote the production and transcription of SOD and GSH [31]. Our results also showed that α-mangostin could inhibit ethanol-induced gastric damage by upregulating Nrf2 and HO-1 protein expression. Additionally, Nrf2 and NF-κB pathways intertwine to promote activation of each other [32]. Nrf2 was negatively correlated with the IL-1β, IL-6, and TNF-α, and the expression of iNOS, COX-2, p-P65, IKKα, NLRP3, and caspase-1. Furthermore, α-mangostin inhibited NLRP3 inflammasome-mediated apoptosis by the NF-κB pathway [33]. Upon stimulation, IKKs can phosphorylate IκB, and then NF-κB p65 is phosphorylated and translocated into the nucleus, and regulates IL-6, IL-1β, and TNF-α releases and promotes the expression of COX-2, iNOS, NLRP3, and caspase-1 proteins [34]. In our study, α-mangostin reduced IL-1β, IL-6, and TNF-α by suppressing the activition of the NF-κB signaling pathway and downstream protein NLRP3/caspase-1. These results indicate that α-mangostin may play a protective role by regulating the activity of Nrf2/HO-1 and NF-κB pathways and inhibiting the activation of NLRP3 inflammasome in the gastric tissues of rats.

An imbalance in the gut flora is crucial for the pathogenesis of ethanol-induced GU. Dysregulation of gut microbiota and disruption of host symbiosis may be important features of ethanol-induced GU, accompanied by the absence of beneficial flora and dissemination of pathogenic bacteria. In our study, α-mangostin treatment increased the abundance of beneficial bacteria, such as *Ligilactobacillus* and *Muribaculum*. *Ligilactobacillus* is an intestinal-dominant bacterium that regulates intestinal immunity and has the potential to alleviate various gastrointestinal disorders [35]. *Muribaculum* is associated with SCFA formation. SCFAs, including propionic acid and butyric acid, are important metabolites produced by intestinal bacteria to maintain intestinal homeostasis, promote the development of regulatory T cells (Tregs), and influence the secretion of cytokines, such as IL-1, IL-6, and TNF-α [36]. Our results showed that α-mangostin significantly increased the propionic acid and butyric acid contents, indicating that α-mangostin promoted the production of SCFAs and reconstructed the disordered gut microbiome.

In conclusion, as shown in Supplementary Fig. S5, the present study demonstrated that α-mangostin has a protective effect against ethanol-induced GU in rats and in an *in vitro* model. The possible mechanism of action is that α-mangostin can inhibit oxidative stress and inflammatory responses, and remodel the balance of intestinal flora by activating the Nrf2/HO-1 pathway, modulating autophagy, inhibiting NF-κB/NLRP3/caspase-1 pathway, and promoting the production of SCFAs. This study provides novel evidence of the use of α-mangostin in GU treatment.

5. Conclusion

This study demonstrated that α-mangostin flavin exerts gastroprotective effects, alleviates oxidative stress and inflammatory responses by modulating the Nrf2/HO-1 and NF-κB/NLRP3/caspase-1 signaling pathways, and regulates the expression of autophagy-related proteins, abundance of intestinal flora, and SCFA levels. This study demonstrates for the first time that α-mangostin has the potential to be used in the treatment of GU by modulating the gut flora and SCFA levels.

In subsequent studies, the role and molecular mechanism α-mangostin in protecting gastric mucosa needs to be further investigated in depth. For example, the related pathway inhibitors can be used at the cellular level to verify the exact role of the NF-κB/NLRP3/caspase-1 signaling pathway. In addition, the mechanism and application of α-mangostin in regulating the intestinal flora to protect the gastric mucosa is also an intriguing direction.

Data availability statement

The raw sequencing data has been deposited into the SRA database in the National Center for Biotechnology Information (NCBI) with the accession number PRJNA1050380.

Ethics declarations

All animal treatments were approved by the Animal Ethics Committee of South-Central Minzu University (2021-scuec-027). All institutional and national guidelines for the care and use of laboratory animals were followed.

CRediT authorship contribution statement

Suqin Yang: Visualization, Validation, Methodology, Investigation, Data curation. **Gang Liu:** Validation, Resources, Investigation. **Xiankun xia:** Validation, Investigation. **Dali Gan:** Validation, Investigation. **Shijian Xiang:** Funding acquisition. **Meixian Xiang:** Writing – original draft, Project administration, Funding acquisition, Conceptualization.

Declaration of competing interest

The authors declare that they have no known competing financial interests or personal relationships that could have appeared to influence the work reported in this paper.

Acknowledgments

This work was supported by the Knowledge Innovation Program of Wuhan-Basic Research (No.2022020201010402), Fundamental Research Funds for the Central Universities, South-Central University for Nationalities (No. CZY21001, No. CZZ21011, No. SYCXJJ382), and Fundamental Research Funds for the Health Commission of Hubei Province (No. ZY2023M022).

The authors acknowledge Qiyuan Su from the Department of Statistics, University of Illinois at Urbana-Champaign, Urbana (United States), for data analysis and manuscript revision.

List of abbreviations

CA	*Camellia atrophy*
COX-2	cyclooxygenase 2
GSH	glutathione
H_2O_2	hydrogen peroxide
HO-1	heme oxygenase 1
iNOS	inducible nitric oxide synthase
IKK	inhibitor of nuclear factor kappa-B kinase
LBT	Lichuan black tea
LC3	microtubule-associated protein light chain 3
IL-1β	interleukin-1β
MDA	malondialdehyde
Nrf2	nuclear factor (erythroid-derived 2)-like 2
NLRP3	NLR family pyrin domain containing 3
NF-κB	nuclear factor κB
PGE2	prostaglandin E2
ROS	reactive oxygen species
SOD	superoxide dismutase
TNF-α	tumor necrosis factor-α.

Appendix A. Supplementary data

Supplementary data to this article can be found online at https://doi.org/10.1016/j.heliyon.2024.e24339.

References

[1] L. Cai, C. Zhao, X. Cao, M. Lu, N. Li, Y. Luo, Y. Wang, Y. Zhao, Chinese herb pollen derived micromotors as active oral drug delivery system for gastric ulcer treatment, Bioact. Mater. 32 (2024) 28–36, https://doi.org/10.1016/j.bioactmat.2023.09.009.

[2] N.B. Ali, S.S. Abdelhamid Ibrahim, M.A. Alsherbiny, E. Sheta, R.A. El Shiekh, R.M. Ashour, A.A. El Gazar, G.M. Ragab, S.H. El Gayed, C.G. Li, E. Abdel Sattar, Gastroprotective potential of red onion (Allium cepa L.) peel in ethanol-induced gastric injury in rats: involvement of Nrf2/HO-1 and HMGB-1/NF-κB trajectories, J. Ethnopharmacol. 319 (Pt 1) (2024) 117115, https://doi.org/10.1016/j.jep.2023.117115.

[3] E. Gugliandolo, M. Cordaro, R. Fusco, A.F. Peritore, R. Siracusa, T. Genovese, R. D'Amico, D. Impellizzeri, R. Di Paola, S. Cuzzocrea, R. Crupi, Protective effect of snail secretion filtrate against ethanol-induced gastric ulcer in mice, Sci. Rep. 11 (1) (2021) 3638, https://doi.org/10.1038/s41598-021-83170-8.

[4] T. Chavan, A. Muth, The diverse bioactivity of α-mangostin and its therapeutic implications, Future Med. Chem. 13 (19) (2021) 1679–1694, https://doi.org/10.4155/fmc-2021-0146.

[5] O.D. John, A.T. Mushunje, N. Surugau, R.M. Guad, The metabolic and molecular mechanisms of α-mangostin in cardiometabolic disorders (review), Int. J. Mol. Med. 50 (3) (2022), https://doi.org/10.3892/ijmm.2022.5176.

[6] R.S. Aziz, A. Siddiqua, M. Shahzad, A. Shabbir, N. Naseem, Oxyresveratrol ameliorates ethanol-induced gastric ulcer via downregulation of IL-6, TNF-α, NF-κB, and COX-2 levels, and upregulation of TFF-2 levels, Biomed. Pharmacother. 110 (2019) 554–560, https://doi.org/10.1016/j.biopha.2018.12.002.

[7] Q.Q. Qiao, Q.B. Luo, S.K. Suo, Y.Q. Zhao, C.F. Chi, B. Wang, Preparation, characterization, and cytoprotective effects on HUVECs of Fourteen novel angiotensin-I-converting enzyme inhibitory peptides from protein hydrolysate of tuna processing by-products, Front. Nutr. 9 (2022) 868681, https://doi.org/10.3389/fnut.2022.868681.

[8] T. Günbatan, İ. Gürbüz, E. Bedir, A.M. Gençler Özkan, Ö. Özçınar, Investigations on the anti-ulcerogenic activity of sideritis caesarea H. Duman, aytaç & başer, J. Ethnopharmacol. 258 (2020) 112920, https://doi.org/10.1016/j.jep.2020.112920.

[9] D.Y. Lee, M.Y. Song, K.S. Hong, S.M. Yun, Y.M. Han, E.H. Kim, Low dose administration of mature silkworm powder induces gastric mucosa defense factors in ethanol-induced gastric injury rat model, Food Sci. Biotechnol. 32 (11) (2023) 1551–1559, https://doi.org/10.1007/s10068-023-01278-1.

[10] M. Ghasemzadeh Rahbardar, B.M. Razavi, H. Hosseinzadeh, Investigating the ameliorative effect of alpha-mangostin on development and existing pain in a rat model of neuropathic pain, Phytother Res. 34 (12) (2020) 3211–3225, https://doi.org/10.1002/ptr.6768.

[11] E.C.S. da Silva, G.C. Bernardo Guerra, E.R.D. de Araújo, J. Schlamb, V.C. da Silva, E. de Aragão Tavares, R. Dantas-Medeiros, L.S. Abreu, J. Fechine Tavares, R. F. de Araújo Júnior, D. Esposito, M. Moncada, S. Maria Zucolotto, Phenolic-rich extract of Nopalea cochenillifera attenuates gastric lesions induced in

experimental models through inhibiting oxidative stress, modulating inflammatory markers and a cytoprotective effect, Food Funct. 14 (7) (2023) 3242–3258, https://doi.org/10.1039/d2fo03735a.
[12] R. Wang, F. Sun, C. Ren, L. Zhai, R. Xiong, Y. Yang, W. Yang, R. Yi, C. Li, X. Zhao, Hunan insect tea polyphenols provide protection against gastric injury induced by HCl/ethanol through an antioxidant mechanism in mice, Food Funct. 12 (2) (2021) 747–760, https://doi.org/10.1039/d0fo02677h.
[13] R. Liu, Y.T. Hao, N. Zhu, X.R. Liu, J.W. Kang, R.X. Mao, C. Hou, Y. Li, The gastroprotective effect of small molecule oligopeptides isolated from walnut (juglans regia L.) against ethanol-induced gastric mucosa injury in rats, Nutrients 12 (4) (2020), https://doi.org/10.3390/nu12041138.
[14] Y.T. Mohamed, I.A. Naguib, A.A. Abo Saif, M.H. Elkomy, B.S. Alghamdi, W.R. Mohamed, Role of ADMA/DDAH-1 and iNOS/eNOS signaling in the gastroprotective effect of tadalafil against indomethacin-induced gastric injury, Biomed. Pharmacother. 150 (2022) 113026, https://doi.org/10.1016/j.biopha.2022.113026.
[15] K. Pohl, P. Moodley, A.D. Dhanda, Alcohol's impact on the gut and liver, Nutrients 13 (9) (2021), https://doi.org/10.3390/nu13093170.
[16] C. Xie, J. Teng, X. Wang, B. Xu, Y. Niu, L. Ma, X. Yan, Multi-omics analysis reveals gut microbiota-induced intramuscular fat deposition via regulating expression of lipogenesis-associated genes, Anim Nutr 9 (2022) 84–99, https://doi.org/10.1016/j.aninu.2021.10.010.
[17] X. Li, R. Gui, X. Wang, E. Ning, L. Zhang, Y. Fan, L. Chen, L. Yu, J. Zhu, Z. Li, L. Wei, W. Wang, Z. Li, Y. Wei, X. Wang, Oligosaccharides isolated from Rehmannia glutinosa protect LPS-induced intestinal inflammation and barrier injury in mice, Front. Nutr. 10 (2023) 1139006, https://doi.org/10.3389/fnut.2023.1139006.
[18] S.L. Zheng, Y.Z. Wang, Y.Q. Zhao, W.Y. Zhu, C.F. Chi, B. Wang, High Fischer ratio oligopeptides from hard-shelled mussel: preparation and hepatoprotective effect against acetaminophen-induced liver injury in mice, Food Biosci. 53 (2023), https://doi.org/10.1016/j.fbio.2023.102638.
[19] M.F. Wu, Q.H. Xi, Y. Sheng, Y.M. Wang, W.Y. Wang, C.F. Chi, B. Wang, Antioxidant peptides from monkfish swim bladders: ameliorating NAFLD in vitro by suppressing lipid accumulation and oxidative stress via regulating, AMPK/Nrf2 Pathway 21 (6) (2023), https://doi.org/10.3390/md21060360.
[20] Y. Jing, Y. Yu, F. Bai, L. Wang, D. Yang, C. Zhang, C. Qin, M. Yang, D. Zhang, Y. Zhu, J. Li, Z. Chen, Effect of fecal microbiota transplantation on neurological restoration in a spinal cord injury mouse model: involvement of brain-gut axis, Microbiome 9 (1) (2021) 59, https://doi.org/10.1186/s40168-021-01007-y.
[21] P.S. Tu, Y.T. Tung, W.T. Lee, G.C. Yen, Protective effect of Camellia oil (Camellia oleifera abel.) against ethanol-induced acute oxidative injury of the gastric mucosa in mice, J. Agric. Food Chem. 65 (24) (2017) 4932–4941, https://doi.org/10.1021/acs.jafc.7b01135.
[22] Y. Xia, N. Liu, X. Xie, G. Bi, H. Ba, L. Li, J. Zhang, X. Deng, Y. Yao, Z. Tang, B. Yin, J. Wang, K. Jiang, Z. Li, Y. Choi, F. Gong, X. Cheng, J.J. O'Shea, J.J. Chae, A. Laurence, X.P. Yang, The macrophage-specific V-ATPase subunit ATP6V0D2 restricts inflammasome activation and bacterial infection by facilitating autophagosome-lysosome fusion, Autophagy 15 (6) (2019) 960–975, https://doi.org/10.1080/15548627.2019.1569916.
[23] D. Wu, M. Cao, N. Li, A. Zhang, Z. Yu, J. Cheng, X. Xie, Z. Wang, S. Lu, S. Yan, J. Zhou, J. Peng, J. Zhao, Effect of trimethylamine N-oxide on inflammation and the gut microbiota in Helicobacter pylori-infected mice, Int Immunopharmacol 81 (2020) 106026, https://doi.org/10.1016/j.intimp.2019.106026.
[24] Y. Ge, X. Xu, Q. Liang, Y. Xu, M. Huang, α-Mangostin suppresses NLRP3 inflammasome activation via promoting autophagy in LPS-stimulated murine macrophages and protects against CLP-induced sepsis in mice, Inflamm. Res. 68 (6) (2019) 471–479, https://doi.org/10.1007/s00011-019-01232-0.
[25] A.M. Pisoschi, A. Pop, The role of antioxidants in the chemistry of oxidative stress: a review, Eur. J. Med. Chem. 97 (2015) 55–74, https://doi.org/10.1016/j.ejmech.2015.04.040.
[26] S. Yang, F. Zhou, Y. Dong, F. Ren, α-Mangostin induces apoptosis in human osteosarcoma cells through ROS-mediated endoplasmic reticulum stress via the WNT pathway, Cell Transplant. 30 (2021) 9636897211035080, https://doi.org/10.1177/09636897211035080.
[27] G. Filomeni, E. Desideri, S. Cardaci, G. Rotilio, M.R. Ciriolo, Under the ROS.thiol network is the principal suspect for autophagy commitment, Autophagy 6 (7) (2010), https://doi.org/10.4161/auto.6.7.12754.
[28] K.R. Parzych, D.J. Klionsky, An overview of autophagy: morphology, mechanism, and regulation, Antioxid Redox Signal 20 (3) (2014) 460–473, https://doi.org/10.1089/ars.2013.5371.
[29] M.E. Sánchez Mendoza, Y. López Lorenzo, L. Cruz Antonio, A. Cruz Oseguera, J. García Machorro, J. Arrieta, Gastroprotective effect of juanislamin on ethanol-induced gastric lesions in rats: role of prostaglandins, nitric oxide and sulfhydryl groups in the mechanism of action, Molecules 25 (9) (2020), https://doi.org/10.3390/molecules25092246.
[30] S.Y. Zhang, Y.Q. Zhao, Y.M. Wang, X.R. Yang, C.F. Chi, B. Wang, Gelatins and antioxidant peptides from Skipjack tuna (Katsuwonus pelamis) skins: purification, characterization, and cytoprotection on ultraviolet-A injured human skin fibroblasts, Food Biosci. 50 (2022), https://doi.org/10.1016/j.fbio.2022.102138.
[31] M. Talebi, M. Talebi, T. Farkhondeh, G. Mishra, S. İlgün, S. Samarghandian, New insights into the role of the Nrf2 signaling pathway in green tea catechin applications, Phytother Res. 35 (6) (2021) 3078–3112, https://doi.org/10.1002/ptr.7033.
[32] Y.M. Wang, X.Y. Li, J. Wang, Y. He, C.F. Chi, B. Wang, Antioxidant peptides from protein hydrolysate of skipjack tuna milt: purification, identification, and cytoprotection on H_2O_2 damaged human umbilical vein endothelial cells, Process Biochem 113 (2022) 258–269, https://doi.org/10.1016/j.procbio.2022.01.008.
[33] J. Chen, M. Bian, L. Pan, H. Yang, α-Mangostin protects lipopolysaccharide-stimulated nucleus pulposus cells against NLRP3 inflammasome-mediated apoptosis via the NF-κB pathway, J. Appl. Toxicol. 42 (9) (2022) 1467–1476, https://doi.org/10.1002/jat.4306.
[34] K.K. Nyati, K. Masuda, M.M.U. Zaman, P.K. Dubey, D. Millrine, J.P. Chalise, M. Higa, S. Li, D.M. Standley, K. Saito, H. Hanieh, T. Kishimoto, TLR4-induced NF-κB and MAPK signaling regulate the IL-6 mRNA stabilizing protein Arid5a, Nucleic Acids Res. 45 (5) (2017) 2687–2703, https://doi.org/10.1093/nar/gkx064.
[35] J. Lukasik, T. Dierikx, I. Besseling van der Vaart, T. de Meij, H. Szajewska, Multispecies probiotic for the prevention of antibiotic-associated diarrhea in children: a randomized clinical trial, JAMA Pediatr. 176 (9) (2022) 860–866, https://doi.org/10.1001/jamapediatrics.2022.1973.
[36] S. Deleu, K. Machiels, J. Raes, K. Verbeke, S. Vermeire, Short chain fatty acids and its producing organisms: an overlooked therapy for IBD? EBioMedicine 66 (2021) 103293 https://doi.org/10.1016/j.ebiom.2021.103293.